Geoderma Regional 34 (2023) e00683

Contents lists available at ScienceDirect

Geoderma Regional

journal homepage: www.elsevier.com/locate/geodrs

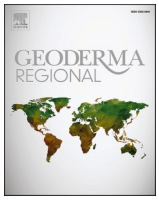

Tamarugite, $NaAl(SO_4)_2{\cdot}6H_2O$, as a valuable indicator of soil degradation in a Spanish coastal wetland receiving acidic leachates from spilled mine waste

Juan Carlos Fernández-Caliani

Department of Earth Sciences, Faculty of Experimental Sciences, University of Huelva, Campus de El Carmen, 21071 Huelva, Spain

ARTICLE INFO

Keywords:
Tamarugite
Pyrite
Acid sulfate soil
Salt efflorescence
Tidal wetland
Huelva estuary

ABSTRACT

This paper documents the first occurrence of tamarugite in a Spanish coastal wetland registered as a UNESCO Biosphere Reserve, and discusses its origin and environmental significance. Tamarugite occurs as bladed crystals in efflorescent coatings on the topsoil of marshy areas, alongside an abandoned mining railroad. Tamarugite formation is described as a sequential process involving: (1) Oxidative dissolution of pyrite ore spilled on the former railway tracks and generation of acidic sulfate-rich waters; (2) decomposition of layer minerals under acidic conditions and release of Al^{3+} ions into solution; (3) interaction between acid discharges and estuarine water during flood tidal periods; and (4) precipitation of tamarugite and associated sulfate salts (sideronatrite, epsomite, pickeringite) under strongly evaporative conditions. These transient minerals have potential to release acid and associated major elements (Al, Fe, Mg, Na, S) and trace metals (e.g. Zn) into the solution causing detrimental effects. The occurrence of tamarugite is, therefore, a valuable indicator of environmental degradation in wetland ecosystems.

1. Introduction

Tamarugite is a hydrated double sulfate of sodium and aluminum, with chemical formula ideally $NaAl(SO_4)_2{\cdot}6H_2O$, which crystallizes in a monoclinic structure (space group $P2_1/a$) built up from nearly regular octahedra $[Al(OH)_6]^{3+}$ and double-stranded chains $[Na(SO_4)_2]_3$ extending along [001] (Mereiter, 2013). It is a relatively rare mineral named after its discovery locality at Pampa del Tamarugal (Atacama desert, Chile), where it forms part of a suite of secondary, water-soluble sulfate minerals found in the weathered zone of sulfide ore deposits. In these acidic environments, tamarugite is usually formed by reaction of acid sulfate solutions with alkali-rich aluminous rocks.

Although most occurrences of tamarugite have been reported from arid environments, it has also been found at coastal localities with moderately high rainfall, with sodium supplied from sea-spray (Segnit, 1976; King, 1998; Garvie, 1999). Tamarugite is also an acidic by-product of pyrite oxidation in drastically disturbed or drained acid sulfate soils (Fitzpatrick et al., 2008, Fitzpatrick et al., 2010a,Fitzpatrick et al., 2010b; Raven et al., 2010) and, less commonly in salt efflorescence from acid mine drainage affected systems (Harris et al., 2003; Valente et al., 2016). Other occurrences are linked to active geothermal systems, due to acidic volcanic waters or low-temperature gaseous emanations (fumaroles) reacting with the host rocks (Lombardi and Sposato, 1981; Mackenzie et al., 1995; Delmelle and Bernard, 2000; Baltatzis et al., 2001). Tamarugite has been reported in cavities across the world (Hill and Forti, 1997; Frau and Da Pelo, 1999; Puscas et al., 2013).

This paper documents the first occurrence of tamarugite in a coastal wetland system severely polluted by metal-mining related wastes and industrial effluents. The study was undertaken with a two-fold objective: firstly, to explain the origin of tamarugite in certain marshy areas of the wetland; and secondly, to evaluate its potential use as a mineral indicator to assist in the identification of sulfidic materials in estuaries impacted by legacy mining pollution.

2. Environmental setting

The study area is situated in the west side of the middle estuary of Huelva (Fig. 1), which is formed by the junction of the rivers Odiel and Tinto on the southwestern coastline of Spain. It has a Mediterranean climate with Atlantic influence, characterized by hot, dry summers and mild winters. The average annual rainfall is about 525 mm, and the mean temperature ranges from 11.0 °C in winter to 25.8 °C in summer. The estuary has a mesotidal regime with a mean tidal range of 2.1 m

E-mail address: caliani@uhu.es.

https://doi.org/10.1016/j.geodrs.2023.e00683
Received 24 April 2023; Received in revised form 28 June 2023; Accepted 4 July 2023
Available online 6 July 2023

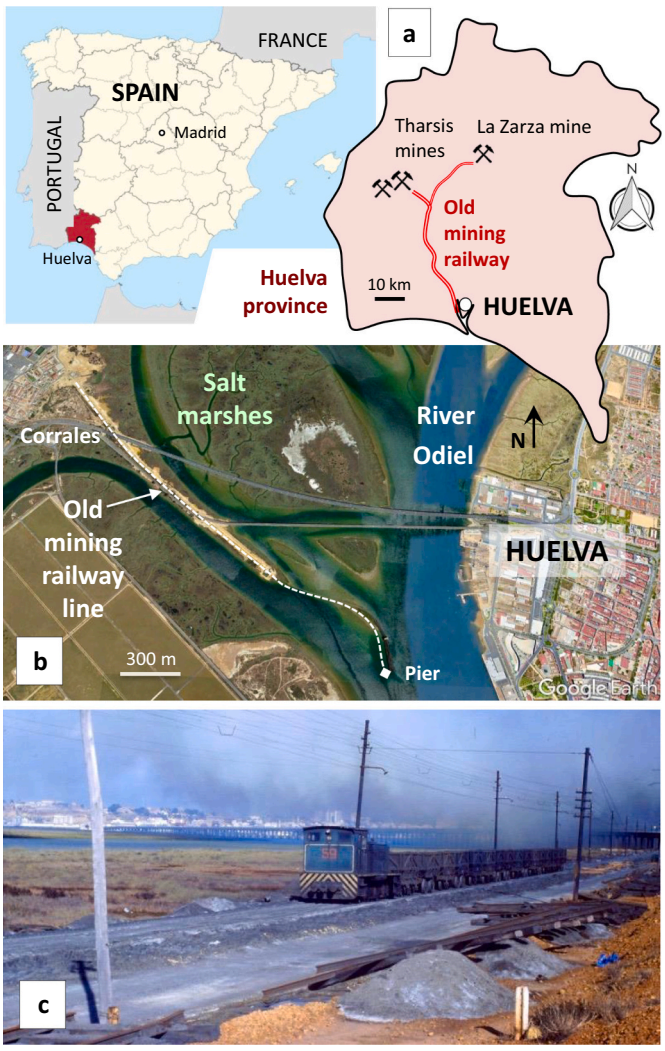

Fig. 1. Locality map showing the old railway line of the Tharsis mines (a). The study area is located on the western bank of the salt marshes of the Odiel River (b), along the last section of the former railway corridor (c), where an uncontrolled quantity of pyrite ore was stockpiled on the ground and spilled from the mining rail cars (photo *ca.* 1970, Aljaraque Municipality Archive).

(Carro et al., 2019), but high spring tides and extreme high waters may lead to episodic flooding events. The estuarine marsh soil classifies as a Tidalic Stagnic Solonchak (Humic) in accordance with the IUSS Working Group WRB (2015). It was formed on fluvio-marine silty-clayey sediments primarily composed of quartz, illite, kaolinite and feldspars (Fernández-Caliani et al., 1997) and sustains a vegetative cover of salt-tolerant plants. These salt marshes form part of a coastal wetland declared in 1983 as a Biosphere Reserve by UNESCO.

It is noteworthy that the estuarine environment is heavily impacted by multiple contamination sources, including natural and anthropogenic contributions. It receives acid discharges from natural processes (acid rock drainage) and from abandoned mine sites (acid mine drainage) in the mineralized catchment area (Nelson and Lamothe, 1993; Galán et al., 2003). In addition, industrial effluents have been discharged directly into the estuary after six decades of intense industrial activity along the river banks (Sáinz et al., 2004), with Cu, Pb, Zn, As, Cd, and Hg being the pollutants most commonly reported (Fernández-Caliani et al., 1997).

While considerable work has been done over decades to characterize the detrimental effects of acid mine drainage and industrial discharges on water and sediment chemistry (see Pérez-López et al., 2023, for a recent review), very few studies have addressed the connection between hazardous pollutants and pyrite ore rail transport and port loading operations (Grantcharova and Fernández-Caliani, 2022; Gallego and Fernández-Caliani, 2023). These studies showed a high degree of soil contamination arising from past mine railway activities. The sulfidic material spilled on the tracks of the old railroad that linked the mines of Tharsis and La Zarza to the Huelva estuary is a historic point-source of acid and heavy metals to the nearby salt marshes of the Odiel River, where the Tharsis Sulphur and Copper Company constructed a pier opposite the city of Huelva (Fig. 1b) for overseas shipment of pyrite ore concentrates.

After the closing of the mines in the late 1990s, the railway tracks and the rail-port link facilities were abandoned and dismantled after providing mineral transport services for more than a century. During the years when the railway was operating, one could see alongside the railroad tracks large quantities of pyrite ores stockpiled on ground and spilled from operational incidents while being transported (Fig. 1c). In recent years, the last section of the former rail line was converted into a gravel-surfaced trail for cycling and walking. However, the underlying soil retains a considerable degree of residual contamination by arsenic and heavy metals that pose a very high ecological risk (Gallego and Fernández-Caliani, 2023).

3. Material and methods

The surface precipitates, here referred to as salt efflorescences, were collected randomly at four sampling sites (T1, T2, T3, and T4) along the stretch of the former railway line that lies between Corrales station and the old mineral loading dock (Fig. 2a). These soils classify as Tidalic Spolic Technosol (Salic, Thionic) in accordance with IUSS Working Group WRB, 2015 (Table 1). Efflorescence salt samples weighing a minimum of 0.1 kg were scraped from the soil surface layer using a stainless steel trowel and transferred to the laboratory in sealed, airtight polyethylene bags. Additionally, one sample (P1) of the soil embankment subjected to pyrite ore cargo spills (Fig. 2b) was taken for analysis. This soil classifies as a Spolic Technosol (Hyperartefactic Sulfidic Thionic) in accordance with IUSS Working Group WRB, 2015 (Table 1).

After air-drying, the samples were gently ground by hand in an agate mortar. Soil pH was measured with a digital pH meter calibrated with two buffer solutions at pH 4 and 7, in a soil to deionized water suspension of 1:2.5 (*w/v*), after shaking for 15 min and left to stand for 30 min. Mineralogical characterization of tamarugite was carried out using a combination of analytical methods, including powder X-ray diffraction (XRD), field emission scanning electron microscopy (FESEM) coupled with energy dispersive X-ray spectrometry (EDS), and thermogravimetric (TGA) and differential thermogravimetric (DTG) analysis.

Phase identification was performed on random powder mounts by XRD with a BRUKER AXS D8-Advance diffractometer, operating in the Bragg-Brentano configuration with monochromatic Cu-Kα radiation under standard instrumental conditions: step scanned from 3 to 65° 2θ, with a step size of 0.02° and a counting time of 0.6 s per step, at 30 mA and 40 kV. The XRD patterns were recorded with the DifraccPlus software (BRUKER AXS) and compared with reference patterns from the JCPDS database. The program UnitCell (Holland and Redfern, 1997) was used for the refinement of unit-cell parameters from powder-diffraction data by a nonlinear least-squares fitting procedure.

A selection of hand-picked specimens clean of visual impurities were dehydrated, coated with sputtered carbon and examined by FESEM using a JEOL JSM-IT500HR instrument coupled to an energy dispersive X-ray spectrometer (EDS) detector (X-Max detector, Oxford Instruments). FESEM images were acquired to visualize textural and micromorphological of the crystals, and compositional data were obtained using a standard-less quantification method. Working distance was set at 10–15 mm, accelerating voltage at 15 kV, and probe current at 2.50 nA.

Thermo-gravimetric analysis was conducted using a Mettler Toledo TG/DSC1 instrument equipped with STARe software. A nearly pure

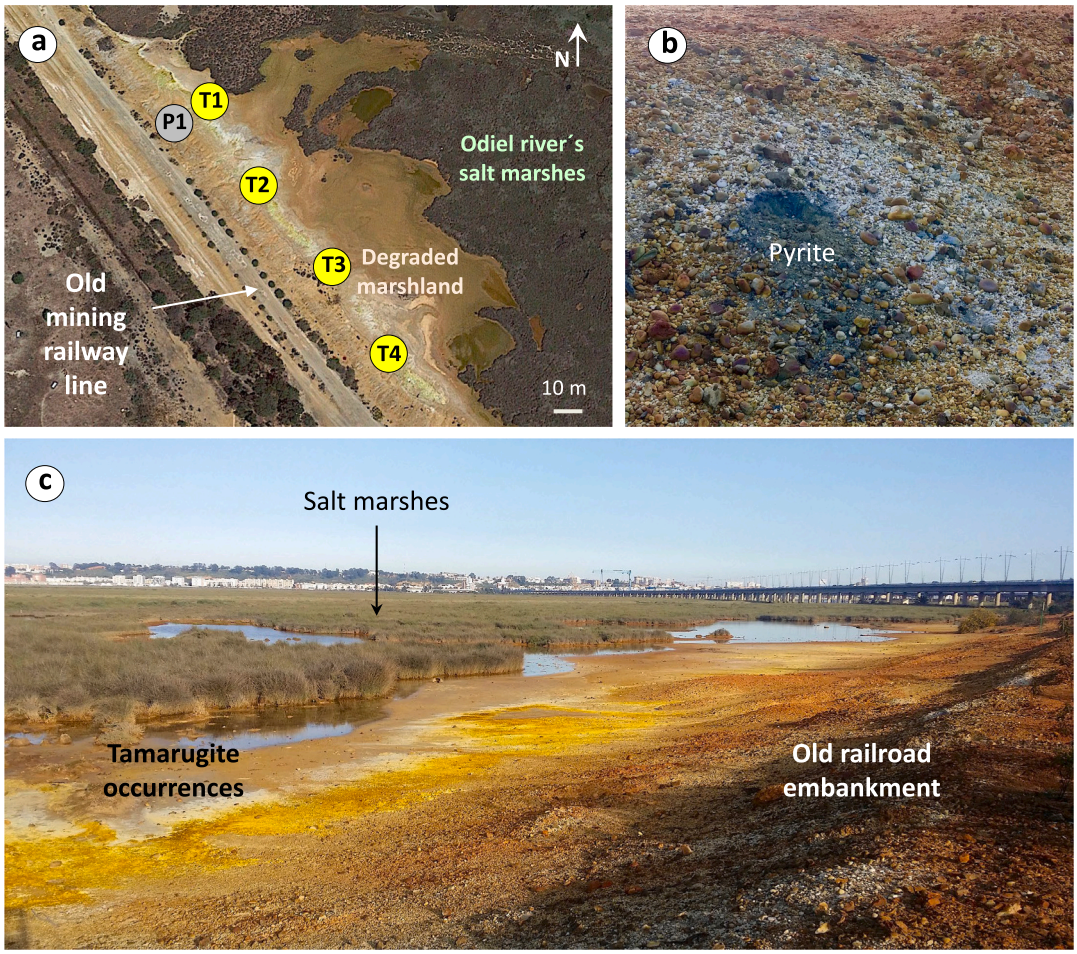

Fig. 2. (a) Aerial view (Google Earth) of the sampling sites and field pictures of the old railroad embankment (b) showing evidence of pyrite ore cargo spills, and (c) tamarugite occurrences on the supra-tidal soil alongside the railway line.

Table 1
Classification of soil profiles in accordance with the World Reference Base for Soil Resources.

Brief description	Site number in Fig. 2a	World Reference Base for Soil Resources (WRB)[1]
Odiel river salt marshes	–	Tidalic Stagnic Solonchak (Humic)
Degraded marshland	T1, T2, T3, T4	Tidalic Spolic Technosol[2] (Salic, Thionic)
Old mining railway line	P1	Spolic Technosol[2] (Hyperartefactic Sulfidic Thionic)

[1] IUSS Working Group WRB (2015).
[2] Technosol: Soil with strong human influence, containing significant amounts of artefacts.

tamarugite sample was placed into an open alumina crucible and heated in static air from room temperature to 1000 °C. Experimental mass loss (TGA) and the first derivative of mass loss (DTG) curves were obtained at a constant heating rate of 10 °C/min.

4. Results and discussion

4.1. Characterization

The railroad soil impacted by hazardous material cargo spills is extremely acidic in reaction (pH = 2.3) and contains highly reactive sulfidic material along with quartz and layer silicates (mica and kaolinite), together with minor jarosite, feldspars, and gypsum. The FESEM-EDS study of the sulfide-rich material (sample P1) provided evidence of actively oxidizing pyrite with a large amount of etching pits on the crystal surfaces.

Tamarugite occurs as bright yellow efflorescent salts and encrustations about 1 cm thick coating the surface soil of the bare salt marsh alongside the old rail bed, at the base of the embankment (Fig. 2c). During rainy periods this highly soluble efflorescence dissolves and then reappears the next dry period, as reported elsewhere in other tamarugite occurrences (Segnit, 1976; Mackenzie et al., 1995). The efflorescent salts produce acidic solutions upon dissolution in water, with pH values ranging between 3.06 and 3.20.

The powder XRD diagrams of the efflorescent samples (Fig. 3) exhibited well-developed patterns for tamarugite, with strongest lines at 12.6, 4.22, 3.96, 3.65, 3.16, and 2.90 Å spacings that can be assigned to the reflections (020), (−131), (131), (160), (240), and (180), respectively (Robinson and Fang, 1969). A least-squares unit-cell refinement of powder-diffraction data gave the following cell parameters for the monoclinic space group $P2_1/a$: $a = 7.372$ Å; $b = 25.195$ Å; $c = 6.107$ Å; $\beta = 94.84°$; cell volume = 1130.2 Å^3.

Tamarugite was typically mixed with halite and impurities of detrital grains of quartz in all sampling sites, as determined by XRD analysis. Some lower intensity diffraction peaks that match well with the major diffraction lines of the standard data of sideronatrite (sample T1),

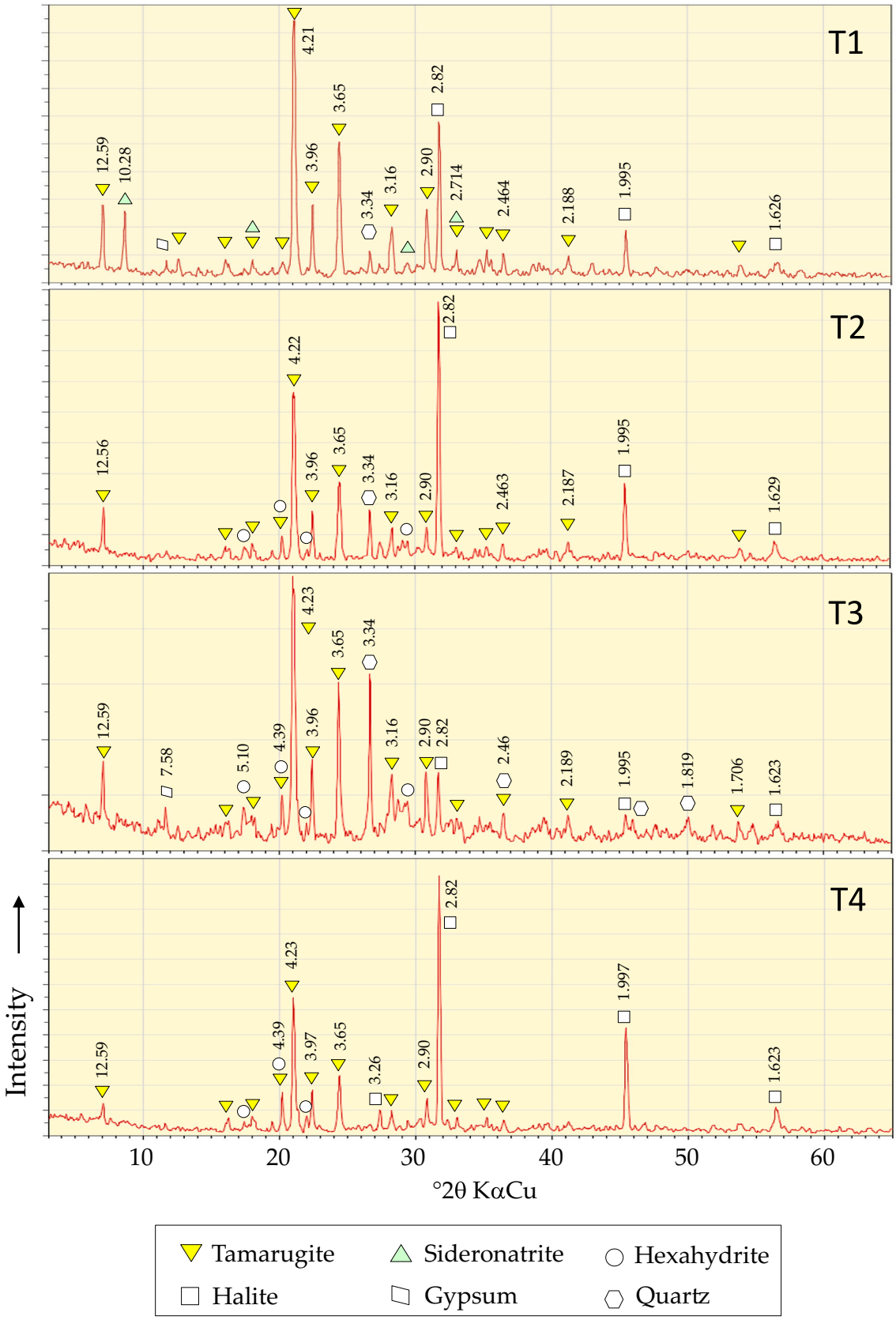

Fig. 3. Powder X-ray diffraction patterns of the salt efflorescence samples consisting of mixtures of tamarugite, halite, and/or sideronatrite, hexahydrite, and gypsum.

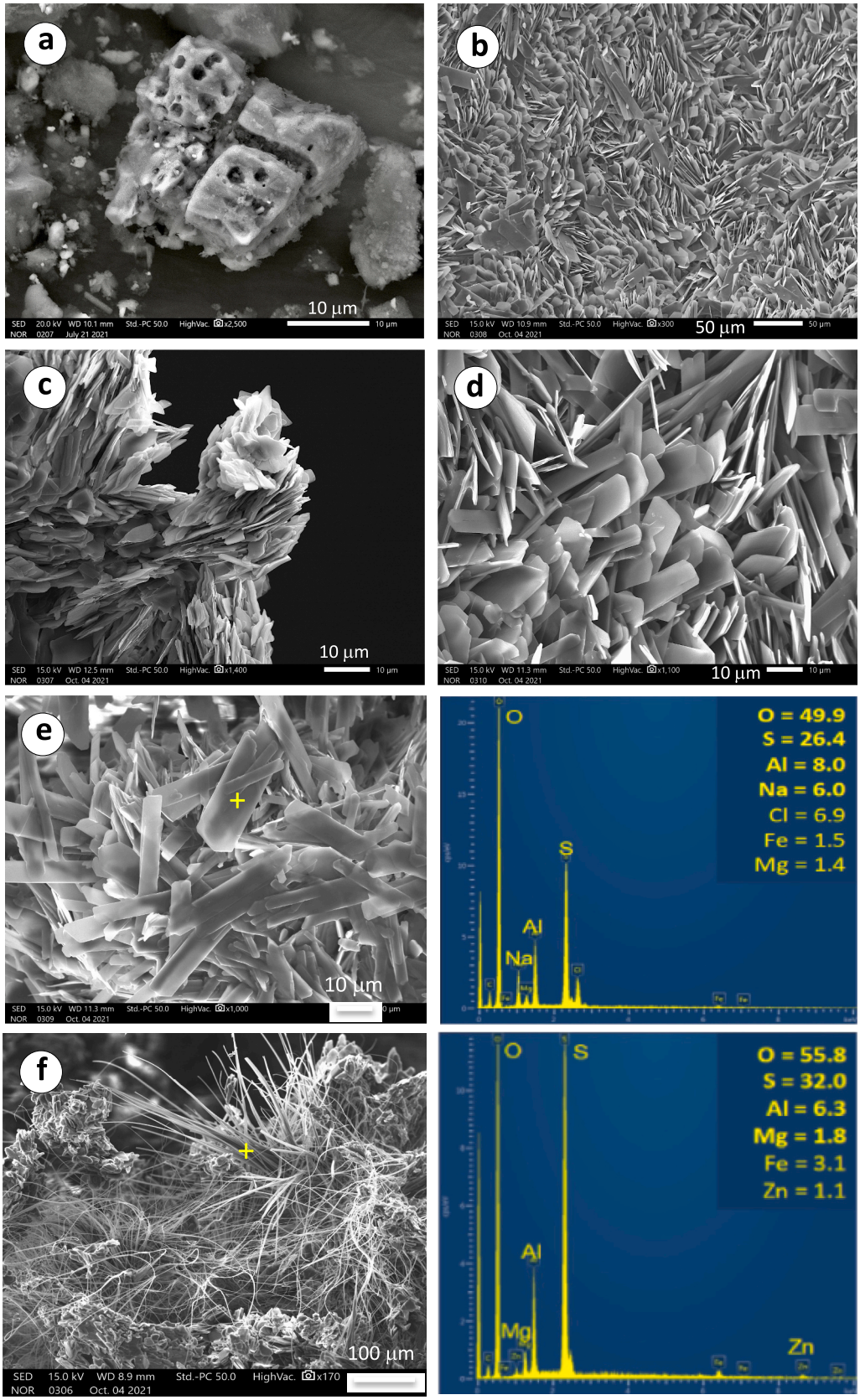

Fig. 4. FESEM secondary electron images showing: (a) a pyrite crystal with dissolution channels and etch pits on surfaces; (b) general view of the evaporative mineral precipitates; (c) tabular and bladed crystals of tamarugite forming rosette-like clusters and (d) displaying a platelet arrangement; (e) chemical analyses (wt%) by EDS of selected single crystals of tamarugite and (f) hair-like pickeringite.

hexahydrite (samples T2, T3, and T4) and gypsum (T1 and T3) were also observed in the XRD patterns.

Tamarugite crystals were not visible to the naked eye. FESEM examination of loose powders (Fig. 4) revealed that they form tightly packed microcrystalline aggregates of bladed or tablet-like crystals flattened parallel to (010). Single euhedral crystals can reach maximum dimensions up to 50 μm, but typically ranging between 10 and 20 μm in length and less than 2 μm wide.

Tamarugite was variable in chemical composition, with S ranging from 22 to 26 wt%, Al from 7.2 to 10.8 wt%, and Na from 6.0 to 11.6 wt %, and traces of Fe and Mg, according to EDS analysis of nine individually chosen crystals. The presence of chlorine (up to 9 wt%) suggests that halite precipitation occurred during the drying process, thus obscuring the actual composition of tamarugite analyzed in loose powder mounts. Although traces of Cu, Zn, and Pb have been reported in tamarugite from other locations (Lombardi and Sposato, 1981), such potentially toxic trace elements were not present at detectable levels in any of the crystals analyzed by EDS. However, the FESEM-EDS study revealed the presence of aggregates of hair-like crystals that appear to be close in composition to pickeringite, which contained traces of Zn and Fe in addition to major elements, namely S, Al and Mg (Fig. 4d).

The results of the thermal analysis (Fig. 5) indicated two major regions of mass loss, with the most significant mass release peaks occurring in the low temperature range of 100–240 °C, due to dehydration in several steps, and in the range of 500–800 °C related to sulfate thermal decomposition (Pelovski et al., 1995). The stepwise loss of the six crystallization water molecules per formula unit of tamarugite took place as follows: The first stage of dehydration occurred at 105 °C, due to initial loss of 1.5 water molecules, and a well-developed dehydration peak occurs at 170 °C corresponding to a mass loss of about 20%. Based on the calculation of the mass loss within the temperature range of 25–240 °C, it can be inferred that approximately 30% of the total sample mass was lost during the controlled heating process. Considering the known stoichiometry and crystal structure of tamarugite, which has a molecular weight of 350.4 g/mol, the mass lost due to dehydration was estimated to be approximately 105 g/mol. This mass loss aligns well with the expected change in mass resulting from the removal of six water molecules associated with each formula unit of tamarugite (Meshram et al., 2019):

$$NaAl(SO_4)_2 \cdot 6H_2O \rightarrow NaAl(SO_4)_2 + 6H_2O$$

The thermal decomposition of the dehydrated phase was observed in two distinct mass loss steps, at 593 °C and 727 °C, during the heating process. The first thermal peak is attributed to the loss of SO_3 resulting from the decomposition of sodium sulfate and the second one could be related to the decomposition of aluminum sulfate, through the following reactions:

$$NaAl(SO_4)_2 \rightarrow \tfrac{1}{2}\, Na_2SO_4 + \tfrac{1}{2}\, Al_2(SO_4)_3$$

$$Na_2SO_4 \rightarrow Na_2O + SO_3$$

$$Al_2(SO_4)_3 \rightarrow Al_2O_3 + 3SO_3$$

The thermal analyses showed that the tamarugite has a thermal behavior similar to that described at other localities (Segnit, 1976; Lombardi and Sposato, 1981).

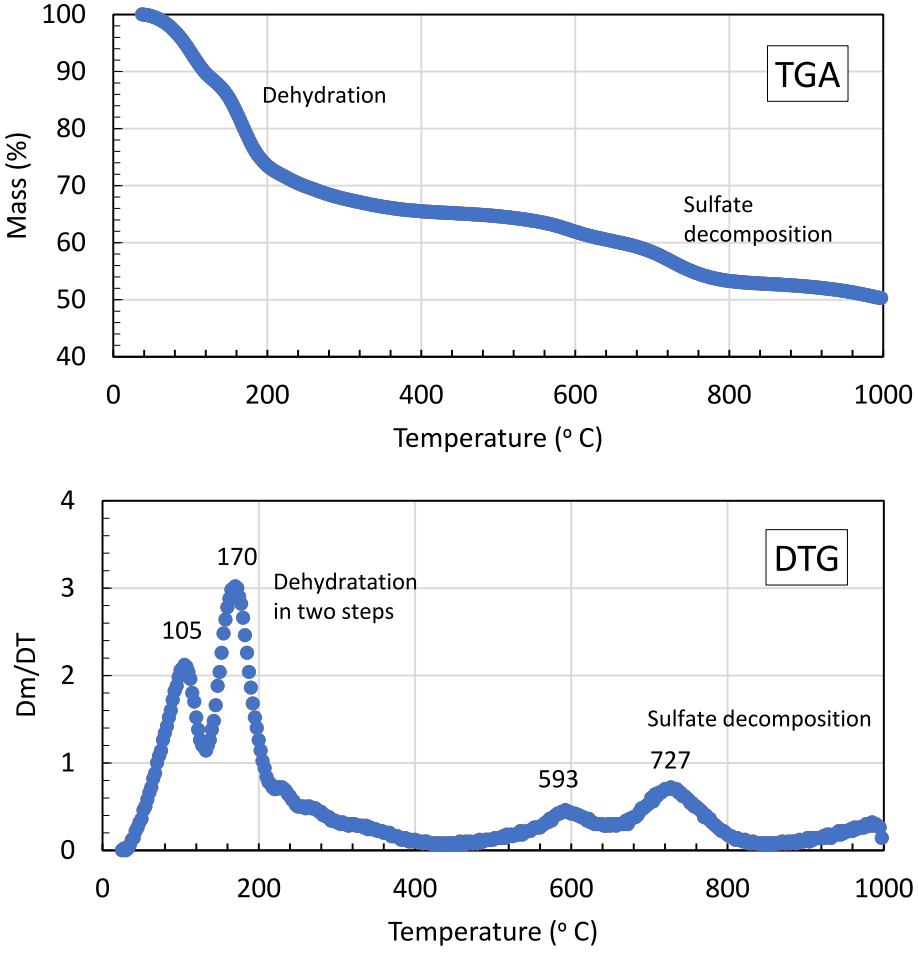

Fig. 5. Curve of mass loss to temperature (TGA) and first-order differentiation (Dm/DT) curve of mass loss as a function of temperature (DTG).

4.2. Origin and environmental significance

In a recent paper (Gallego and Fernández-Caliani, 2023) it has been shown that oxidative dissolution of finely-crushed pyrite ore spilled on the former railway tracks is an important source of acid, sulfate and potentially toxic trace elements to the nearby tidal marsh soils. Chemical corrosion of the remaining pyrite was confirmed by the presence of pitted crystal faces. The overall equation for the complete oxidation of pyrite in humid air can be written as follows:

$$FeS_2 + 15/4O_2 + 7/2H_2O \rightarrow Fe(OH)_3 + 2SO_4^{2-} + 4H^+$$

Hydrogen ions (H^+) released by sulfide oxidation lead to an acidic and oxidizing environment conducive to incongruent dissolution of aluminosilicate minerals, notably layer silicates but also feldspars, thus resulting in the solubilization of additional metal ions into solution, including dissolved aluminum (Al^{3+}) and other cations like K^+, Na^+, Ca^{2+} and Mg^{2+}. Mean concentration of Al in the leachates produced by sulfide waste was estimated to be as high as 848.5 mg L^{-1} in the supratidal marsh of the study area (Dávila et al., 2019). The occurrence of tamarugite is indicative of acidic conditions (Fitzpatrick et al., 2008; Fitzpatrick et al., 2010b; Raven et al., 2010) sufficiently strong to dissolve, at least partially, dioctahedral mica (muscovite/illite) and feldspars (plagioclase) of the argillaceous sediments, releasing Al^{3+} ions into the soil-water system by the reactions:

$$KAl_3Si_3O_{10}(OH)_2 + 10H^+ \leftrightarrow 3H_4SiO_4 + K^+ + 3Al^{3+}$$

$$CaAl_2Si_2O_8 + 8H^+ \leftrightarrow 2H_4SiO_4 + Ca^{2+} + 2Al^{3+}$$

Thus, the three main dissolved constituents in the acid discharges are iron, aluminum, and sulfate, as occurs in acid mine drainage systems (Nordstrom, 2020). Similar processes take place in various other environments where naturally occurring sulfide minerals are oxidized, such as acid sulfate soils in modern inland (Fitzpatrick et al., 2008; Mosley et al., 2014) and coastal (e.g. Fanning et al., 2017) zones.

It is therefore believed that tamarugite was formed from the interaction between estuarine water and acid sulfate solution leached from sulfide-rich materials comprising the spilled pyrite. Acid soil drainage played a key role in delivering dissolved Al^{3+} and sulfate ions from the railway embankment toward the nearby marshland. The supply of Na^+ needed for tamarugite formation is likely to have originated from deposition of wind-blown salt-spray and flooding during spring tides, when the sediments of the supratidal zone are flooded with estuarine water for hours.

The process of crystallization on the soil surface occurred by direct precipitation from the acid brine solution, once this aqueous solution becomes supersaturated with respect to tamarugite, due to increased evaporation especially during the onset of dry periods. The reaction to form tamarugite can be represented as:

$$Al^{3+} + Na^+ + 2SO_4^{2-} + 6H_2O \leftrightarrow NaAl(SO_4)_2 \cdot 6H_2O$$

According to the scenario above, schematically depicted in Fig. 6, the tamarugite-forming process took place under constrained hydrogeochemical and climatic conditions, such as low pH, high availability of aluminum and sodium, and high evaporation rates, which are regarded as the main factors contributing to the progress of the reaction. The occurrence of a well-developed evaporative layer of tamarugite on soil surfaces above mean high water is a clear evidence for acid sulfate soil formation. Additionally, the combination of sulfate ions with alkaline-earth metal cations released by silicate hydrolysis resulted in the formation of various by-products of the sulfate formation process, such as sideronatrite ($Na_2Fe(SO_4)_2(OH) \cdot 3H_2O$), gypsum ($CaSO_4 \cdot 2H_2O$), pickeringite ($MgAl_2(SO_4)_4 \cdot 22H_2O$), and hexahydrite ($MgSO_4 \cdot 6H_2O$) likely formed by dehydration of epsomite ($MgSO_4 \cdot 7H_2O$), through the reactions:

$$Fe^{3+} + 2Na^+ + 2SO_4^{2-} + 4H_2O \leftrightarrow Na_2Fe(SO_4)_2(OH) \cdot 3H_2O + H^+$$

$$Ca^{2+} + SO_4^{2-} + 2H_2O \leftrightarrow CaSO_4 \cdot 2H_2O$$

$$Mg^{2+} + 2Al^{3+} + 4SO_4^{2-} + 22H_2O \leftrightarrow MgAl_2(SO_4)_4 \cdot 22H_2O$$

$$Mg^{2+} + SO_4^{2-} + 7H_2O \leftrightarrow MgSO_4 \cdot 7H_2O$$

$$MgSO_4 \cdot 7H_2O \leftrightarrow MgSO_4 \cdot 6H_2O + H_2O$$

The paragenesis tamarugite-sideronatrite-epsomite-pickeringite-gypsum-halite is consistent with those reported in active acid sulfate

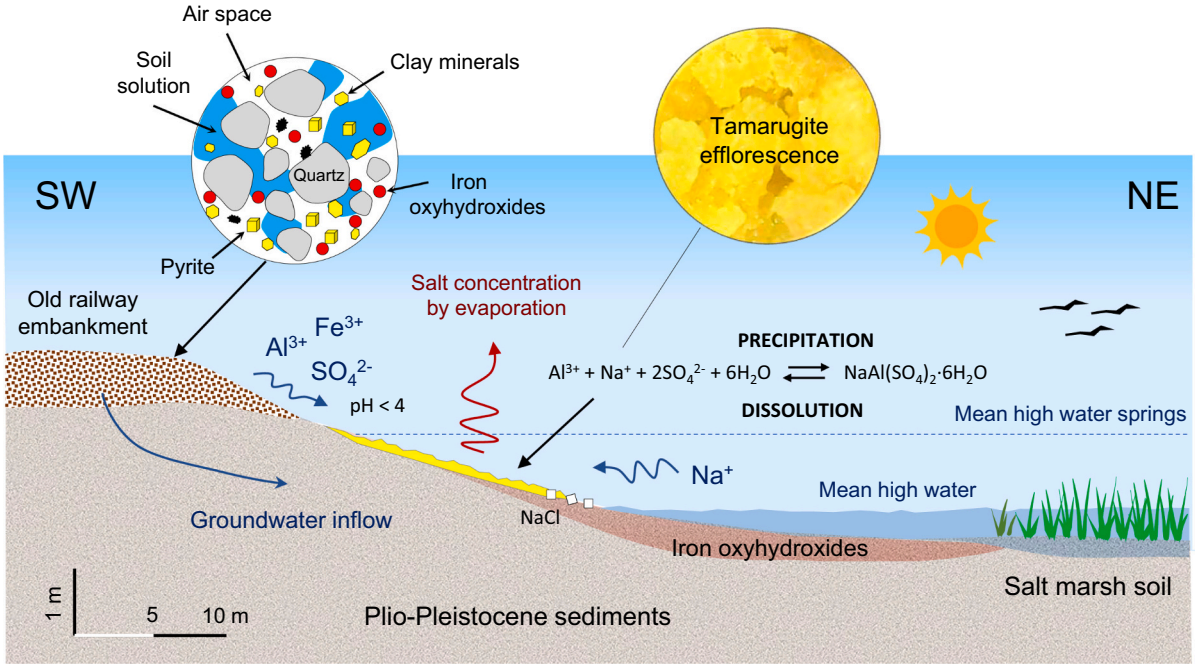

Fig. 6. Schematic cross-section diagram summarizing the depositional realm and the processes involved in the formation of tamarugite efflorescence.

soils (Thomas et al., 2009). The precipitating efflorescent minerals incorporate and remove from the aqueous solution substantial amounts of sulfate, Al, Fe, Na, Mg, and Ca, and may also host some potentially toxic trace elements like Zn, as detected by EDS analysis. It is worth noting that, these salt efflorescences have potential for aerial transport (Fitzpatrick et al., 2010a, 2010b), and consequently may contaminate the ambient air and affect human health, especially when they contain heavy metals (Loredo-Jasso et al., 2021).

Of particular concern is that these highly soluble salts are flushed into receiving estuarine waters during rainfall and flooding tidal periods, resulting in sulfate-rich acidic waters. For each mole, tamarugite may release three moles of stored acidity, as described by the reaction:

$$NaAl(SO_4)_2{\cdot}6H_2O \rightarrow Al(OH)_3 + 3H_2O + 2SO_4^{2-} + 3H^+ + Na^+$$

At low pH values, the buffering is regulated by the hydrolysis of aluminum hydroxide resulting in the release of Al^{3+} ions, which is toxic to many aquatic plants and fish (Shand et al., 2016) and potentially jeopardize the wetland ecosystem.

$$Al(OH)_3 + 3H^+ \leftrightarrow Al^{3+} + 3H_2O$$

Therefore, the transient efflorescent sulfate minerals have an important influence on the chemistry of the receiving estuarine waters at the point of discharge due to precipitation, dehydration and dissolution processes during wetting-drying cycles in the wetland.

5. Conclusions

Oxidizable pyrite ore spilled on ground from the mining rail cars serves as a feedstock for acid sulfate soil development, with exceptional occurrences of tamarugite in marshy areas of the wetland along the former railroad line. The findings from this study support that tamarugite formation can be described as a sequential process comprising various steps: (1) oxidative dissolution of pyrite and generation of acidic sulfate-rich waters; (2) decomposition of accompanying clay minerals under acidic conditions; (3) interaction between acid discharges and estuarine water during flood tidal periods; and (4) precipitation of tamarugite and associated sulfate phases on the supratidal marsh soil under strongly evaporative conditions.

Tamarugite has been proved particularly useful indicator in the identification of residual sulfidic material following exposure to aerobic conditions in legacy pollution sites periodically affected by tidal water. It is an environmental indicator of strongly acid soil reaction and regulates the cycling of Al and Na in the wetland soil receiving leachates from spilled mine waste. As such, future work should involve quantifying the amount of retained acidity from tamarugite using standard acid-base accounting methods. Ultimately, tamarugite and other by-products of the acid sulfate soil formation, notably sideronatrite, epsomite and pickeringite, have potential for acid and metal release during flush flooding events, thus leading to ecosystem deterioration.

Declaration of Competing Interest

The authors declare that they have no known competing financial interests or personal relationships that could have appeared to influence the work reported in this paper.

Data availability

Data will be made available on request.

Acknowledgements

The author acknowledges the reviewers for their constructive comments, especially for suggesting and providing information on the classification of soils in accordance to the World Reference Base for Soil Resources (WRB). Funding for open access charge: Universidad de Huelva / CBUA.

References

Baltatzis, E., Valsami-Jones, E., Magganas, A., Kati, M., 2001. Tamarugite from Milos Island, Greece. Neues Jahrb. Mineral. Monatshefte 8, 371–377.
Carro, B., Borrego, J., Morales, J.A., 2019. Estuaries of the Huelva coast: Odiel and Tinto estuaries (SW Spain). In: Morales, J.A. (Ed.), The Spanish Coastal Systems. Springer Nature, pp. 543–564.
Dávila, J.M., Sarmiento, A.M., Santisteban, M., Luís, A., Fortes, J.C., Díaz-Curiel, J., Valbuena, C., Grande, J.A., 2019. The UNESCO national biosphere reserve (Marismas del Odiel, SW Spain): an area of 18,875 ha affected by mining waste. Environ. Sci. Pollut. Res. 26, 33594–33606.
Delmelle, P., Bernard, A., 2000. Downstream composition changes of acidic volcanic waters discharged into the Banyupahit stream, Ijen caldera, Indonesia. J. Volcanol. Geotherm. Res. 97, 55–75.
Fanning, D.S., Rabenhorst, M.C., Fitzpatrick, R.W., 2017. Historical developments in the understanding of acid sulfate soils. Geoderma 308, 191–206.
Fernández-Caliani, J.C., Ruiz, F., Galán, E., 1997. Clay mineralogy and heavy metal distributions in the lower estuary of Huelva and adjacent Atlantic shelf, SW Spain. Sci. Total Environ. 198, 181–200.
Fitzpatrick, R.W., Shand, P., Marvanek, S., Merry, R.H., Thomas, M., Simpson, S.L., Raven, M.D., McClure, S., 2008. Acid sulfate soils in subaqueous, waterlogged and drained soil environments in Lake Albert, Lake Alexandrina and River Murray below Blanchetown (Lock 1): properties, distribution, genesis, risks and management. CSIRO Land and Water Science Report 46/08. CSIRO, Adelaide 167. https://doi.org/10.4225/08/58597320be185. Available online.
Fitzpatrick, R., Shand, P., Raven, M., McClure, S., 2010a. Occurrence and environmental significance of sideronatrite and other mineral precipitates in acid sulfate soils. In: International Annual Meetings of the Soil Science Society of America; Long Beach, California, USA. Conference Abstract. Available online. https://a-c-s.confex.com/crops/2010am/webprogram/Paper61347.html (accessed 25 June 2023).
Fitzpatrick, R., Shand, P., Raven, M., McClure, S., 2010b. Occurrence and environmental significance of sideronatrite and other mineral precipitates in acid sulfate soils. In: Gilkes, R.J., Prakongkep, N. (Eds.), Proceedings of the 19th World Congress of Soil Science; Soil Solutions for a Changing World; Processes in acid sulfate soil materials; 2010 Aug 1–6. IUSS, Brisbane, Australia, pp. 80–83. Available online. https://www.iuss.org/19th%20WCSS/Symposium/pdf/0540.pdf (accessed 25 June 2023).
Frau, F., Da Pelo, S., 1999. Tamarugite from the gold mine of Furtei, Sardinia, Italy. Mineral. Petrogr. Acta 42, 83–88.
Galán, E., Gómez-Ariza, J.L., González, I., Fernández-Caliani, J.C., Morales, E., Giráldez, I., 2003. Heavy metal partitioning in river sediments severely polluted by acid mine drainage in the Iberian Pyrite Belt. Appl. Geochem. 18, 409–421.
Gallego, L., Fernández-Caliani, J.C., 2023. Pyrite ore cargo spills as a source of soil pollution and ecological risk along the abandoned railway corridors of the Tharsis and Rio Tinto mines (Spain). Environ. Monit. Assess. 195, 97.
Garvie, L.A.J., 1999. Sideronatrite and metasideronatrite efflorescence formed in a coastal sea-spray environment. Mineral. Mag. 63, 757–759.
Grantcharova, M.M., Fernández-Caliani, J.C., 2022. Soil acidification, mineral neoformation and heavy metal contamination driven by weathering of sulphide wastes in a Ramsar wetland. Appl. Sci. 12, 249.
Harris, D.L., Lottermoser, B.G., Duchesne, J., 2003. Ephemeral acid mine drainage at the Montalbion silver mine, North Queensland. Aust. J. Earth Sci. 50, 797–809.
Hill, C.A., Forti, P., 1997. Cave Minerals of the World, 2nd ed. National Speleological Society, Huntsville.
Holland, T.J.B., Redfern, S.A.T., 1997. UNITCELL: a nonlinear least-squares program for cell-parameter refinement implementing regression and deletion diagnostics. J. Appl. Crystallogr. 30, 84.
IUSS Working Group WRB, 2015. World Reference Base for soil resources 2015: International soil classification system for naming soils and creating legends for soil maps. In: World Soil Resources Reports 106. FAO, Rome. Available online. www.fao.org/3/i3794en/I3794en.pdf (accessed 17 April 2023).
King, R.J., 1998. Tamarugite on the Isle of Wight. UK Mineral Mag. 62, 371–372.
Lombardi, G., Sposato, A., 1981. Tamarugite from Vulcano, Aeolian Islands, Italy. Can. Mineral. 19, 403–407.
Loredo-Jasso, A.U., Villalobos, M., Ponce-Pérez, D.B., Pi-Puig, T., Meza-Figueroa, D., Del Rio-Salas, R., Ochoa-Landín, L., 2021. Characterization and pH neutralization products of efflorescent salts from mine tailings of (semi-)arid zones. Chem. Geol. 580, 120370.
Mackenzie, K.M., Rodgers, K.A., Browne, P.R.L., 1995. Tamarugite, $NaAl(SO_4)_2{\cdot}6H_2O$, from Te Kopia, New Zealand. Mineral. Mag. 59, 754–757.
Mereiter, K., 2013. Redetermination of tamarugite, $NaAl(SO_4)_2{\cdot}6H_2O$. Acta Crystallogr. E 69, 63–64.
Meshram, A., Jain, A., Gautam, D., Singh, K.K., 2019. Synthesis and characterization of tamarugite from aluminium dross: part I. J. Environ. Manag. 232, 978–984.
Mosley, L.M., Zammit, B., Jolley, A.M., Barnett, L., Fitzpatrick, R., 2014. Monitoring and assessment of surface water acidification following rewetting of oxidised acid sulfate soils. Environ. Monit. Assess. 186, 1–18.
Nelson, C.H., Lamothe, P.J., 1993. Heavy metal anomalies in the Tinto and Odiel River and estuary system, Spain. Estuaries 16, 496–511.
Nordstrom, D.K., 2020. Geochemical modeling of iron and aluminum precipitation during mixing and neutralization of acid mine drainage. Minerals 10, 547.
Pelovski, Y., Tsankov, M., Petkova, V., Gruncharov, L., 1995. Thermal decomposition of sodium aluminium sulphate crystallohydrate. J. Therm. Anal. 43, 351–357.

Pérez-López, R., Millán, R., Basallote, M.D., Carrero, S., Parviainen, A., Freydier, R., Macías, F., Cánovas, C.R., 2023. Effects of estuarine water mixing on the mobility of trace elements in acid mine drainage leachates. Mar. Pollut. Bull. 187, 114491.

Puscas, C.M., Onac, B.P., Effenberger, H.S., Povara, I., 2013. Tamarugite-bearing paragenesis formed by sulphate acid alteration in Diana cave. Roman. Eur. J. Miner. 25, 479–486.

Raven, M.D., Fitzpatrick, R., Self, P., Shand, P., 2010. Identification and formation of complex hydrated sulfate salts in acid sulfate soils from Australia using advanced XRD techniques. In: Abstract – Invited keynote paper for 2010 International Annual Meetings of the Soil Science Society of America. Symposium - Soil Minerals in Natural and Agroecosystems. October 31 to November 4, 2010. Long Beach, California, p. 97–6. Available online: http://a-c-s.confex.com/crops/2010am/webprogram/Paper57512.html (accessed 25 June 2023).

Robinson, P.D., Fang, J.H., 1969. Crystal structures and mineral chemistry of double-salt hydrates: I. direct determination of the crystal structure of tamarugite. Am. Mineral. 54, 19–30.

Sáinz, A., Grande, J.A., De la Torre, M.L., 2004. Characterisation of heavy metal discharge into the ria of Huelva. Environ. Int. 30, 557–566.

Segnit, E.R., 1976. Tamarugite from Anglesea, Victoria. Australia Mineral Mag. 40, 642–644.

Shand, P., Gotch, T., Love, A., Raven, M., Priestley, S., Grocke, S., 2016. Extreme environments in the critical zone: linking acidification hazard of acid sulfate soils in mound spring discharge zones to groundwater evolution and mantle degassing. Sci. Total Environ. 568, 1238–1252.

Thomas, B.P., Merry, R.H., Creeper, N.L., Fitzpatrick, R., Shand, P., Raven, M.D., Jayalath, N., 2009. Acid sulfate soil assessment of the lower Loddon River and Burnt Creek, Central Victoria. CSIRO Land & Water Science Report CLW. https://doi.org/10.25919/ypzg-3131. Available online.

Valente, T., Grande, J.A., De la Torre, M.L., 2016. Magnesium and aluminum sulfates in salt efflorescences from acid mine drainage in the Iberian Pyrite Belt (SW Spain). In: Drebenstedt, C., Paul, M. (Eds.), Mining Meets Water – Conflicts and Solutions, Proceedings IMWA 2016, Freiberg, Germany, pp. 445–450.